The 8th European Congress on Computational Methods in Applied Sciences and Engineering
ECCOMAS Congress 2022
5–9 June 2022, Oslo, Norway

COMPUTATIONAL MICRO-MAGNETO-MECHANICS – APPLICATION TO THIN FILM COMPOSITES

CHRISTIAN DORN AND STEPHAN WULFINGHOFF

Institute for Materials Science – Computational Materials Science
Kiel University, Kaiserstr. 2, 24143 Kiel, Germany
{cdo,swu}@tf.uni-kiel.de, www.tf.uni-kiel.de/matwis/cms/en

Key words: Coupled Problem, Finite Element Method, Exponential Map, Generalized Standard Material

Abstract. We formulate a material model for micro-magneto-mechanics based on the generalized standard material approach. Our model includes exchange, elastic, anisotropy, demagnetizing and Zeeman energy. Furthermore we account for dissipative micro-magnetic behavior by means of a dissipation potential. For the constrained optimization problem w.r.t. magnetization we rely on the exponential map algorithm. We demonstrate our ideas with numerical examples. In particular we apply our model to a thin film composite. With this composite we represent the magneto-mechanical part of a magneto-electric composite sensor (resp. small sensor segment). Our numerical experiments focus on FeCoSiB as the magnetostrictive material. We discuss the coupling effects for the considered thin film composite in detail.

1 INTRODUCTION

Detecting biomagnetic fields of heart and brain requires highly sensitive magnetic field sensors such as e.g. SQUID magnetometers (superconducting quantum interference device). High cost and technical effort (e.g. for cooling) associated with these devices limits access to magnetic diagnostic facilities. Easy-to-handle and cost-effective alternative sensor concepts are required to make magnetoencephalography and magnetocardiography widely available. Composite magneto-electric thin film sensors are one such alternative [1]. These sensors use a route from magnetic signals via mechanics to electric signals [2]. To further improve sensor performance, it is imperative to reduce noise. In particular noise caused by magnetic processes and interactions within the magnetostrictive material is of interest [3].
To reduce noise we need to understand its origin. High-performance modeling and simulation of micro-magneto-mechanics can make a valuable contribution in this respect. To approach modeling of micro-magneto-mechanical materials, the generalized standard material (GSM) framework [9, 10] offers great potential. The multitude of energy contributions governing magneto-mechanics can easily be incorporated. Previously Miehe et al. [13], Miehe and Ethiraj [7] and Ethiraj et al. [8] have adopted this approach. From the GSM framework a constrained optimization problem arises (norm 1 constraint for magnetization). A similar constraint, which occurs for the director in shell theory, was addressed by Simo et al. [4, 5] using the exponential map algorithm. The idea was used in micro-magnetics by Lewis and Nigam [6] and Miehe and

Ethiraj [7]. In order to set up our material model and lay the foundation for the investigation of magnetic noise we follow these two ideas (GSM, exponential map).

2 GEOMETRY AND KINEMATICS

We consider a material volume $V \subset \Omega$ embedded in free space Ω with outward facing normals $\boldsymbol{n}$ resp. $\boldsymbol{N}$, see Fig. 1. Furthermore we denote by $[0,T] \subset \mathbb{R}$ the time range. We are

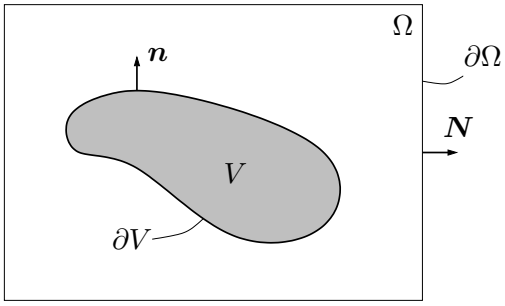

Figure 1: Material volume V embedded in free space Ω

interested in the following three field quantities: displacement $\boldsymbol{u}$, scalar magnetic potential φ and magnetization $\boldsymbol{m}$

$$\boldsymbol{u} : V \times [0,T] \to \mathbb{R}^3 \qquad (\boldsymbol{x},t) \mapsto \boldsymbol{u}(\boldsymbol{x},t) \tag{1}$$

$$\varphi : \Omega \times [0,T] \to \mathbb{R} \qquad (\boldsymbol{x},t) \mapsto \varphi(\boldsymbol{x},t) \tag{2}$$

$$\boldsymbol{m} : V \times [0,T] \to \mathcal{S}^2 \qquad (\boldsymbol{x},t) \mapsto \boldsymbol{m}(\boldsymbol{x},t) \quad \text{with} \quad \|\boldsymbol{m}\| = 1 \tag{3}$$

where $\mathcal{S}^2$ denotes the unit sphere in $\mathbb{R}^3$. Hence we are interested in solving a coupled problem which comprises mechanics, vacuum magnetics and material magnetics. We describe the kinematics of deformation within the small strain setting using the symmetric displacement gradient

$$\boldsymbol{\varepsilon} = \frac{1}{2}\left(\nabla \boldsymbol{u} + (\nabla \boldsymbol{u})^{\top}\right) \tag{4}$$

and moreover assume an additive decomposition of strain $\boldsymbol{\varepsilon}$

$$\boldsymbol{\varepsilon} = \boldsymbol{\varepsilon}^{\mathrm{e}} + \boldsymbol{\varepsilon}^{\mathrm{m}} + \boldsymbol{\varepsilon}^{\star} \tag{5}$$

into an elastic contribution $\boldsymbol{\varepsilon}^{\mathrm{e}}$, a magnetostrictive part $\boldsymbol{\varepsilon}^{\mathrm{m}}$ and an eigenstrain contribution $\boldsymbol{\varepsilon}^{\star}$. As indicated in Eq. (3), the kinematics of the magnetization vector $\boldsymbol{m}$ are characterized by the constraint to the unit sphere $\mathcal{S}^2$ [6]. We use the rotation vector

$$\theta\boldsymbol{\omega} = \theta_1 \boldsymbol{a}_1 + \theta_2 \boldsymbol{a}_2 \tag{6}$$

to describe the rotation of the magnetization vector $\boldsymbol{m}$ on the unit sphere, see Fig. 2, left. More specifically the rotation vector $\theta\boldsymbol{\omega}$ is used in tandem with the exponential map to update the local coordinate system [6, 7]

$$\{\boldsymbol{a}_1, \boldsymbol{a}_2, \boldsymbol{m}\} \leftarrow \exp(\theta\widehat{\boldsymbol{\omega}})\{\boldsymbol{a}_1, \boldsymbol{a}_2, \boldsymbol{m}\} \tag{7}$$

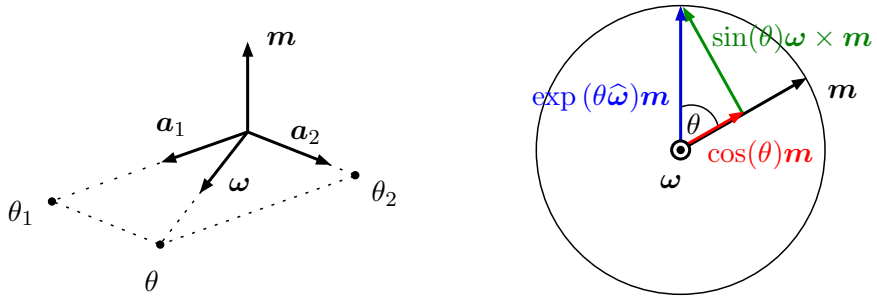

Figure 2: Left: rotation vector $\theta\boldsymbol{\omega}$ in local coordinate system $\{\boldsymbol{a}_1, \boldsymbol{a}_2, \boldsymbol{m}\}$, right: application of exponential map to $\boldsymbol{m}$

where

$$\exp(\theta\widehat{\boldsymbol{\omega}}) = \boldsymbol{\omega}\otimes\boldsymbol{\omega} + \cos(\theta)(\boldsymbol{I} - \boldsymbol{\omega}\otimes\boldsymbol{\omega}) + \sin(\theta)\widehat{\boldsymbol{\omega}} \tag{8}$$

$$\widehat{\boldsymbol{\omega}} = -\boldsymbol{\epsilon}\cdot\boldsymbol{\omega} = -\epsilon_{ijk}\omega_k \boldsymbol{e}_i\otimes\boldsymbol{e}_j \ . \tag{9}$$

We use ϵ_{ijk} to denote the Levi-Civita symbol. An example of an exponential map update is illustrated in Fig. 2, right. By applying the update in Eq. (7) to the magnetization $\boldsymbol{m}$

$$\exp\left(\theta\widehat{\boldsymbol{\omega}}\right)\boldsymbol{m} = \cos(\theta)\boldsymbol{m} + \sin(\theta)\boldsymbol{\omega}\times\boldsymbol{m} \ , \tag{10}$$

we observe that $\boldsymbol{m}$ remains on the unit sphere.

3 GENERALIZED STANDARD MATERIAL FORMULATION

To model the material behavior, we follow the generalized standard material approach [9, 10]. We describe the material behavior by two contributions: the free energy Ψ and the dissipation potential Φ (resp. their volume densities ψ and ϕ). By following the GSM approach, we obtain a material model that automatically fulfills the second law of thermodynamics. In the following we present and briefly discuss the considered energy contributions.
The exchange energy

$$\Psi_{\text{ex}}\left(\nabla\boldsymbol{m}\right) = \int_V A\left\|\nabla\boldsymbol{m}\right\|^2 \mathrm{d}V \tag{11}$$

reflects the exchange interaction between neighboring magnetic moments. This energy contribution represents the propensity of neighboring magnetization vectors $\boldsymbol{m}$ to align with each other. To represent the mechanical behavior of an elastic solid, we include the elastic energy

$$\Psi_{\text{el}}(\boldsymbol{\varepsilon}, \boldsymbol{m}) = \int_V \frac{1}{2}\,\boldsymbol{\varepsilon}^{\text{e}} : \mathbb{C} : \boldsymbol{\varepsilon}^{\text{e}}\,\mathrm{d}V \tag{12}$$

where $\mathbb{C}$ denotes the stiffness tensor (here: isotropic). To express the elastic strain $\boldsymbol{\varepsilon}^{\text{e}}$ in terms of displacement $\boldsymbol{u}$ and magnetization $\boldsymbol{m}$, we use the additive decomposition of strain in Eq. (5).

We further assume that the magnetostrictive strain $\boldsymbol{\varepsilon}^{\mathrm{m}}$ reads [11]

$$\boldsymbol{\varepsilon}^{\mathrm{m}} = \frac{3}{2}\lambda_{\mathrm{s}}\left(\boldsymbol{m}\otimes\boldsymbol{m} - \frac{1}{3}\boldsymbol{I}\right) \tag{13}$$

where λ_{s} denotes the saturation magnetostriction. The next contribution, the anisotropy energy

$$\Psi_{\mathrm{a}}(\boldsymbol{m}) = \int_V K_1\Big(1-(\boldsymbol{m}\cdot\boldsymbol{e}_{\mathrm{a}})^2\Big)\,\mathrm{d}V\ , \tag{14}$$

tends to align magnetization vectors $\boldsymbol{m}$ with a preferential direction (easy axis $\boldsymbol{e}_{\mathrm{a}}$). Here we consider uniaxial anisotropy. In order to reflect the energy of the demagnetizing field $\boldsymbol{H}_{\mathrm{d}} = -\nabla\varphi$ in the material model, we include

$$\Psi_{\mathrm{d}}(\boldsymbol{m},\nabla\varphi) = \int_V \mu_0\nabla\varphi\cdot(M_{\mathrm{s}}\boldsymbol{m})\,\mathrm{d}V - \frac{1}{2}\int_\Omega \mu_0\|\nabla\varphi\|^2\,\mathrm{d}V\ . \tag{15}$$

This energy comprises both the interaction of the demagnetizing field $\boldsymbol{H}_{\mathrm{d}}$ with magnetization $\boldsymbol{m}$ in the material volume V as well as the demagnetizing energy in free space Ω. To represent the interaction of magnetization $\boldsymbol{m}$ with an externally applied field $\boldsymbol{H}'$ we consider the Zeeman energy

$$\Psi_{\mathrm{z}}(\boldsymbol{m}) = \int_V -\mu_0 M_{\mathrm{s}}\boldsymbol{m}\cdot\boldsymbol{H}'\,\mathrm{d}V\ . \tag{16}$$

For the last ingredient of the GSM formulation, the dissipation potential, we assume the form [7]

$$\Phi(\dot{\boldsymbol{m}}) = \int_V \frac{\eta}{2}\dot{\boldsymbol{m}}\cdot\dot{\boldsymbol{m}}\,\mathrm{d}V\ , \tag{17}$$

which reflects the dissipative nature of magnetization changes. All presented energies and potentials contribute to the time continuous rate potential Π

$$\Pi = \dot{\Psi} + \Phi \tag{18}$$

$$= \dot{\Psi}_{\mathrm{ex}}(\nabla\boldsymbol{m}) + \dot{\Psi}_{\mathrm{el}}(\boldsymbol{\varepsilon},\boldsymbol{m}) + \dot{\Psi}_{\mathrm{a}}(\boldsymbol{m}) + \dot{\Psi}_{\mathrm{d}}(\boldsymbol{m},\nabla\varphi) + \dot{\Psi}_{\mathrm{z}}(\boldsymbol{m}) + \Phi(\dot{\boldsymbol{m}})\ . \tag{19}$$

With computational solution in mind, we discretize the time range $[0,T]$ into discrete points $t_0,\dots,t_n,t_{n+1},\dots,T$ with time step $\Delta t = t_{n+1}-t_n$. Furthermore we apply a finite difference scheme to approximate the time derivatives

$$\Pi \approx \frac{\Psi-\Psi_n}{\Delta t} + \Phi\left(\frac{\boldsymbol{m}-\boldsymbol{m}_n}{\Delta t}\right) \tag{20}$$

and obtain the time discrete incremental potential Π_Δ by multiplication with Δt. The stationary points of the incremental potential

$$\Pi_\Delta = \Psi + \Phi_\Delta(\boldsymbol{m}-\boldsymbol{m}_n) \longrightarrow \underset{\boldsymbol{u},\boldsymbol{m},\varphi}{\mathrm{stat}} \tag{21}$$

serve as residuals for the global Newton-Raphson scheme. Note that this is a constrained optimization since $\|\boldsymbol{m}\| = 1$ is required (cf. exponential map Eq. (7) and Fig. 2, right). The variation $\delta_u \Pi_\Delta = 0$ yields the weak form of the linear momentum balance. We obtain the weak form of the Landau-Lifschitz-Gilbert equation [12] (without precession) from $\delta_m \Pi_\Delta = 0$. The variation $\delta_\varphi \Pi_\Delta = 0$ yields the weak form of Gauss' law for magnetism.

4 IMPLEMENTATION AND FINITE ELEMENT METHOD

For solution of the coupled problem we rely on the finite element method (FEM). The computational domain $\Omega \subset \mathbb{R}^3$ is discretized by tetrahedral elements. For the fields of interest we use linear shape functions. In each node we consider six degrees of freedom: displacement (3 dof), scalar magnetic potential (1 dof) and the two angles θ_1 and θ_2 in Eq. (6) (resp. their incremental versions, 2 dof). Residuals and linearizations required for the Newton-Raphson scheme are computed and subsequently implemented by hand.
We use the finite element program ParFEAP 8.6.1j (MPI parallel version of FEAP) in tandem with PETSc 3.13.2. Restarted GMRES preconditioned with block Jacobi (default) and BiCGSTAB preconditioned with block Jacobi showed a favorable behavior for the solution of the linear system.

5 NUMERICAL EXAMPLES

In this section we discuss two examples illustrating the coupling of magnetics and mechanics in our material model. To this end we focus on the magnetostrictive material FeCoSiB ($(Fe_{90}Co_{10})_{78}Si_{12}B_{10}$). An (estimated) parameter set for FeCoSiB is given in Tab. 1, left. For

Table 1: Left: estimated FeCoSiB parameters, right: estimated substrate parameters

A	$1.5 \cdot 10^{-11}\ \frac{\mathrm{J}}{\mathrm{m}}$	η	$1 \cdot 10^{-5}\ \frac{\mathrm{J \cdot s}}{\mathrm{m}^3}$
M_s	$1.5 \cdot 10^{6}\ \frac{\mathrm{A}}{\mathrm{m}}$	λ_s	$30 \cdot 10^{-6}$
K_1	$3 \cdot 10^{2}\ \frac{\mathrm{J}}{\mathrm{m}^3}$	λ	172 GPa
$\boldsymbol{e}_\mathrm{a}$	$\boldsymbol{e}_1$	μ	54 GPa

λ	150 GPa
μ	50 GPa

the two numerical examples we consider a magneto-mechanical thin film on top of a mechanical substrate. An (estimated) parameter set for the substrate is displayed in Tab. 1, right. The film-substrate assembly is embedded in a free space box, see Fig. 4, left. We initialize the magnetization $\boldsymbol{m}$ of the magneto-mechanical thin film according to Fig. 4, right. For external loading by eigenstrain $\boldsymbol{\varepsilon}^\star$ resp. by applied magnetic field $\boldsymbol{H}'$ we use the ramp function illustrated in Fig. 3.

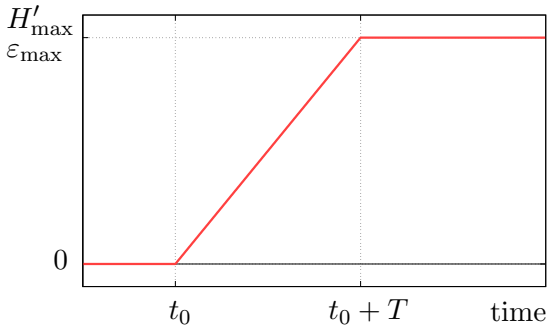

Figure 3: Loading function for applied field $\boldsymbol{H}'$ ($t_0 = 1 \cdot 10^{-9}\,\mathrm{s}$, $T = 1 \cdot 10^{-7}\,\mathrm{s}$, $H'_{\max} = 5 \cdot 10^{-2}\,\mathrm{A/\mu m}$) resp. eigenstrain $\boldsymbol{\varepsilon}^\star$ ($t_0 = 1 \cdot 10^{-9}\,\mathrm{s}$, $T = 1 \cdot 10^{-9}\,\mathrm{s}$, $\varepsilon_{\max} = 0.5\,\%$)

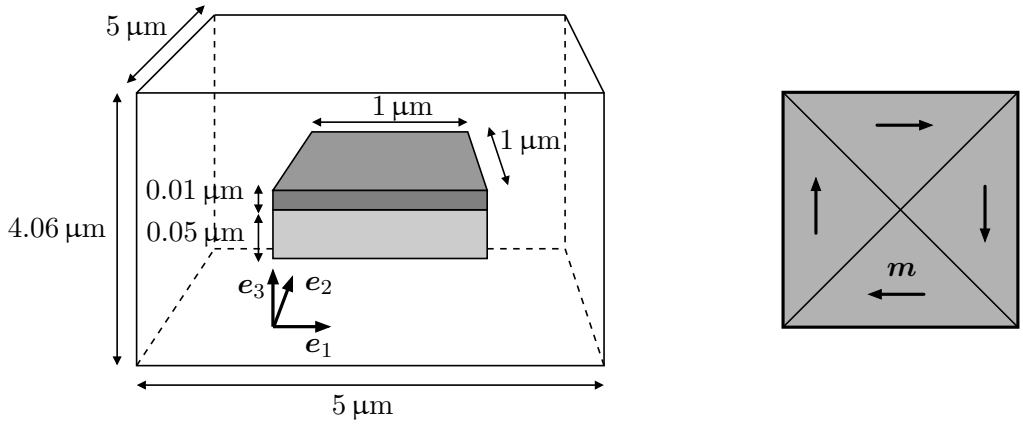

Figure 4: Left: magneto-mechanical film (dark gray) on mechanical substrate (light gray) embedded in free space box, right: initialization of magnetization $\boldsymbol{m}$

5.1 Mechanics influences micro-magnetics

In this first example we illustrate the influence of the mechanical problem on the magnetic problem. To this end we apply an eigenstrain $\boldsymbol{\varepsilon}^\star$ and observe the effect on the magnetic potential φ and the magnetization $\boldsymbol{m}$. We prescribe the eigenstrain $\boldsymbol{\varepsilon}^\star$ in the magneto-mechanical thin film according to

$$\boldsymbol{\varepsilon}^\star \mathrel{\widehat{=}} \begin{bmatrix} \varepsilon(t) & & \\ & -\nu\varepsilon(t) & \\ & & -\nu\varepsilon(t) \end{bmatrix} \tag{22}$$

where $\varepsilon(t)$ follows the ramp function given in Fig. 3 (with $t_0 = 1 \cdot 10^{-9}\,\mathrm{s}$, $T = 1 \cdot 10^{-9}\,\mathrm{s}$, $\varepsilon_{\max} = 0.5\,\%$). We display the results in Fig. 5. The top row shows the relaxed state (just before loading begins). We observe very little deformation and small normal stress σ_{11} in 1-direction (horizontal). Magnetically the structure is in a low energy state that avoids demagnetizing field (4 domain cross state). The bottom row of Fig. 5 illustrates the final state (eigenstrain at maximum value $\varepsilon_{\max}$). As a result of the eigenstrain, the film elongates in 1-direction (horizontal). Since the substrate is not subject to eigenstrain, it resists the elongation of the film. This results

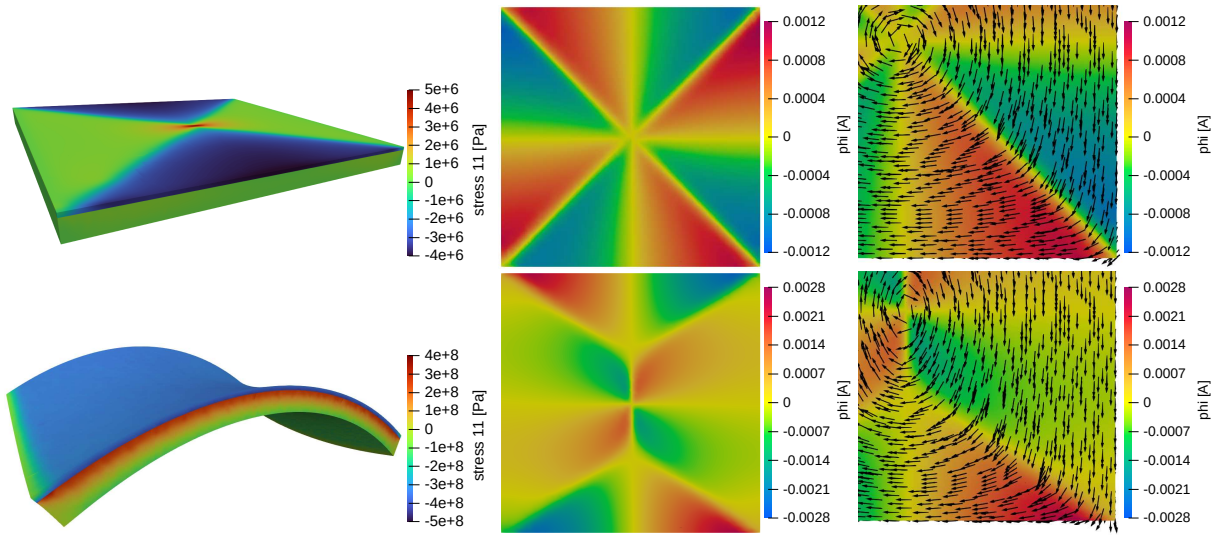

Figure 5: Top row: relaxed state at $t = 1 \cdot 10^{-9}\,\mathrm{s}$, bottom row: final state at $t = 2.2 \cdot 10^{-9}\,\mathrm{s}$, left: stress σ_{11}, warped by displacement $\boldsymbol{u}$ with factor 25, center: scalar magnetic potential φ, right: magnified lower right quarter, φ with magnetization vectors $\boldsymbol{m}$ ($\boldsymbol{m}$ only for every 7th node to improve visibility)

in free deformation of the film at the top free surface and restricted deformation at the shared surface with the substrate. Hence the film-substrate assembly bends. Moreover this mode of deformation leads to compressive stress σ_{11} in the film and tensile stress σ_{11} in the substrate. In Fig. 5, bottom center and right, we observe that the resulting stress-induced anisotropy in 2-direction (vertical) has strong influence on the magnetic potential φ and the magnetization $\boldsymbol{m}$. Thus, the mechanical loading has influenced the magnetic state.

5.2 Micro-magnetics influences mechanics

With this second example we showcase the impact of the magnetic problem on the mechanical problem. The idea is to apply an external magnetic field $\boldsymbol{H}'$ and study the resulting displacement $\boldsymbol{u}$ and stress σ_{11}. We apply the following external magnetic field

$$\boldsymbol{H}' = H'(t)\boldsymbol{e}_1 \tag{23}$$

where $H'(t)$ is characterized by the ramp function in Fig. 3 (with $t_0 = 1 \cdot 10^{-9}\,\mathrm{s}$, $T = 1 \cdot 10^{-7}\,\mathrm{s}$, $H'_{\max} = 5 \cdot 10^{-2}\,\mathrm{A/\mu m}$). Fig. 6 depicts the results. The top row shows again the relaxed state (just before load onset). This state is equivalent to the relaxed state in Fig. 5 and included here to facilitate the comparison to the bottom row. Note that due to the large warp factor the displacement is discernible in Fig. 6, top right. The bottom row in Fig. 6 displays the final state with maximum applied field $H'_{\max}$. On account of the applied field $\boldsymbol{H}'$ the magnetization $\boldsymbol{m}$ is mostly aligned in 1-direction (horizontal). This alignment leads to a magnetostrictive strain $\boldsymbol{\varepsilon}^{\mathrm{m}}$ in 1-direction, cf. Eq. (13). The film elongates in 1-direction and the substrate restricts the free deformation at the shared surface. As a result the film-substrate assembly bends. Furthermore we again observe compressive stress σ_{11} in the film and tensile stress σ_{11} in the substrate. Hence, the magnetic loading has influenced the mechanical state.

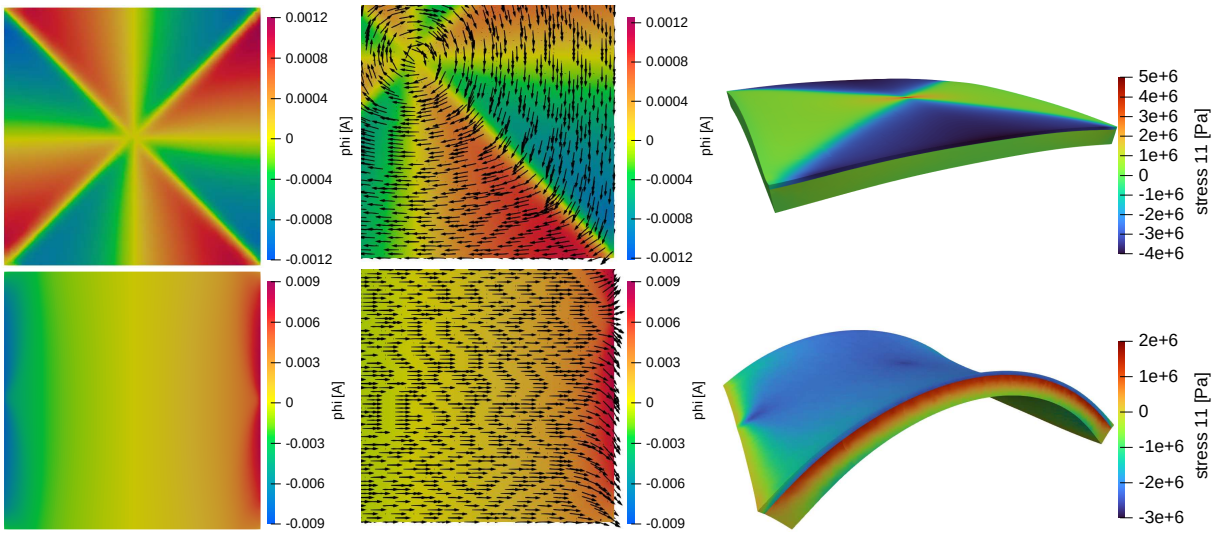

Figure 6: Top row: relaxed state at $t = 1 \cdot 10^{-9}$ s, bottom row: final state at $t = 1.8 \cdot 10^{-7}$ s, left: scalar magnetic potential φ, center: magnified lower right quarter, φ with magnetization vectors $\boldsymbol{m}$ ($\boldsymbol{m}$ only for every 7th node to improve visibility), right: stress σ_{11}, warped by displacement $\boldsymbol{u}$ with factor 5000

We want to make two additional remarks. Firstly, note that stress-induced anisotropy similar to the above example in section 5.1 occurs here as well. This anisotropy would align magnetization $\boldsymbol{m}$ in 2-direction (vertical). However, the applied field $\boldsymbol{H}'$ is sufficiently strong to overcome this effect. Second note: the magnetization $\boldsymbol{m}$ is not fully aligned in 1-direction (horizontal). To achieve more stringent alignment, a stronger applied field $\boldsymbol{H}'$ would be required. However, to illustrate the micro-magneto-mechanical coupling, the chosen setup is adequate.

6 CONCLUSIONS

In this work we have showcased a material model for micro-magneto-mechanics. The model formulation as a generalized standard material ensures thermodynamically consistent material behavior. We include exchange, elastic, anisotropy, demagnetizing and Zeeman energy to represent conservative behavior. Dissipative magnetic behavior is reflected in the dissipation potential. We approach the constrained optimization w.r.t. magnetization using the exponential map algorithm.
We have demonstrated our material model with two numerical examples which show that the coupling of micro-magnetics and mechanics is working well. Our reliable and physically plausible material model provides the basis for investigation of noise caused by magnetic processes and interactions. In future work we intend to study the interaction of domain walls and defects (geometric imperfections, surface roughness, local eigenstrains).

ACKNOWLEDGMENT

This research is funded by the Deutsche Forschungsgemeinschaft (DFG, German Research Foundation) – project number 286471992 within CRC 1261.

REFERENCES

[1] Röbisch, V. et al. Pushing the detection limit of thin film magnetoelectric heterostructures. *Journal of Materials Research* (2017) **32.6**:1009-1019

[2] Viehland, D. et al. Magnetoelectric magnetic field sensors. *Mrs Bulletin* (2018) **43.11**:834-840

[3] Durdaut, P. et al. Phase Noise of SAW Delay Line Magnetic Field Sensors. *Sensors* (2021) **21.16**:5631.

[4] Simo, J.C. and Fox, D.D. On a stress resultant geometrically exact shell model. Part I: Formulation and optimal parametrization. *Computer Methods in Applied Mechanics and Engineering* (1989) **72**:267–304

[5] Simo, J., Fox, D.D. and Rifai, M.S. On a stress resultant geometrically exact shell model. Part III: Computational aspects of the nonlinear theory. *Computer Methods in Applied Mechanics and Engineering* (1990) **79.1**:21–70

[6] Lewis, D. and Nigam, N. Geometric integration on spheres and some interesting applications. *Journal of Computational and Applied Mathematics* (2003) **151**:141–170

[7] Miehe, C. and Ethiraj, G. A geometrically consistent incremental variational formulation for phase field models in micromagnetics. *Computer methods in applied mechanics and engineering* (2012) **245**:331–347

[8] Ethiraj, G., Sridhar, A. and Miehe, C. Variational modeling and homogenization in dissipative magneto-mechanics. *GAMM-Mitteilungen* (2015) **38.1**:75–101

[9] Halphen, B. and Nguyen, Q.S. Generalized standard materials. *Journal de Mécanique* (1975) **14**:39–63

[10] Miehe, C. A multi-field incremental variational framework for gradient-extended standard dissipative solids. *Journal of the Mechanics and Physics of Solids* (2011) **59**:898–923

[11] Hubert, A. and Schäfer, R. *Magnetic Domains: The Analysis of Magnetic Microstructures.* Springer, 3rd edition, (2009).

[12] Gilbert, T.L. A phenomenological theory of damping in ferromagnetic materials. *IEEE transactions on magnetics* (2004) **40.6**:3443–3449

[13] Miehe, C., Rosato, D. and Kiefer, B. Variational principles in dissipative electro-magneto-mechanics: a framework for the macro-modeling of functional materials. *International Journal for Numerical Methods in Engineering* (2011) **86.10**:1225-1276